Graduate Journal of Interdisciplinary Research, Reports & Reviews
(Grad.J.InteR[3])
ark:/85846/JPR3.2023AR.0102035

ISSN(E): 2584-2919
Vol.1, No.1 (2023)
pp.33-40

Research Article

Nanodosimetry-A Study Using The Monte Carlo Code PENELOPE For The TG 6.2 of EURADOS WG 6

L. F. Araújo [*1] and T. C. F. Fonseca [2,3]

[1]*Department of Nuclear Engineering - School of Engineering, Federal University of Minas Gerais (UFMG), Belo Horizonte 31270-901, Minas Gerais, Brazil.* ,
Email: lucasfaraujo@ufmg.br (corresponding author) ,
ORCID: 0000-0001-6837-6213

[2]*Department of Nuclear Engineering - School of Engineering, Federal University of Minas Gerais (UFMG), Belo Horizonte 31270-901, Minas Gerais, Brazil.,*
Email: tcff01@gmail.com ,
ORCID: 0000-0003-2388-5174

[3]*Nuclear Technology Development Center, Belo Horizonte 31270-901, Minas Gerais, Brazil.*

(Received:11-08-23; Accepted:18-10-23)

ABSTRACT:
Background: New technological developments have been made to measure absorbed dose on a small scale, especially at the micro- and nanoscale. Studies have been carried out with short-range ionizing radiation and low-energy particles in human cells to analyze the effect and response of DNA.
Purpose: In this work, a scenario in which a radioactive ^{125}I irradiating several spheres of liquid water were simulated using the EURADOS exercise for computer-aided dosimetry.
Methods: The modelling and simulations were performed with PENELOPE Monte Carlo simulation code. The energy deposited on the targets was used for calculation and analysis.
Results: The obtained results were within acceptable uncertainties of up to 2% in all simulated cases. The average deviation of the results for the two different collisions configurations and the average deviation of the uncertainties obtained in the liquid water targets were 2.5% and 21%, respectively.
Conclusions: The code response was appropriate for the simulated deposited energies in the liquid water sphere, which showed a behavior curve in all configurations and quantitative differences with respect to the first target for different types of collisions.

KEYWORDS: Nanodosimetry, Monte Carlo Simulation, PENELOPE, Low Energy Electrons

1. Introduction

The application of micro- and nanodosimetry is particularly important for the study of cell and DNA damage caused by ionizing radiation. Since the effects of radiation are highly dependent on the spatial distribution of energy deposition at the micro- and nanoscale, the use of advanced dosimetry and modeling techniques is crucial to accurately understand and quantify the risks associated with radiation exposure [1]-[3]. Several studies have been published investigating the effects of ionizing radiation on DNA strand damage and repair mechanisms, which have important implications for cancer therapy and radiation protection strategies [4]-[9]. Some studies have focused primarily on low-energy particles or/and low-range electrons with the aim of understanding the microdosimetric and radio-biological effects of radiation in organic tissues [10]-[14]. The ability to accurately model and simulate the spatial distribution of energy deposition at the

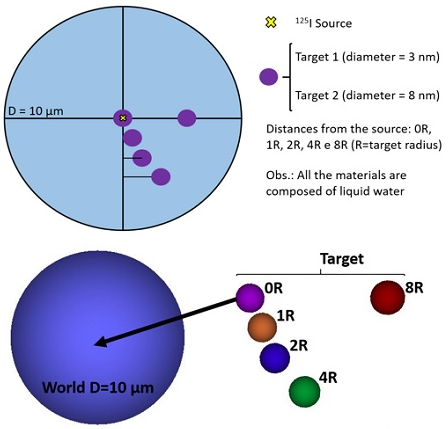

Figure 1: 2D and 3D scheme of MC model for case of nanodosimetry. Source: Vilagrasa et al. 2018 [24].

micro- and nanoscale has the potential to improve our understanding of the underlying mechanisms that drive DNA damage and repair, ultimately leading to more effective cancer treatments and radiation protection protocols [15]-[16]. Monte Carlo codes (MC) facilitate the development of potential theories by using cross-sections to simulate the transport of multiple particles with different kinetic energies, allowing the modeling of geometries at the macro and micrometer levels. Over time, it became necessary to upgrade the codes to meet increasingly specific requirements, especially as they moved from the macro to the micro and nano scales. This upgrade is necessary to meet changing requirements [12]. Several studies can be found in the literature in which MC codes were used to simulate the behaviour of ionizing radiation at the micro and nanoscale [9], [16] - [23]. The "EURADOS (European Radiation Dosimetry) Working Group "Computational Dosimetry" published in 2018 a paper reporting a studying quantifying the contribution to the uncertainty of micro and nanodosimetric simulation results arising from the use of different electron-impact cross-sections, and hence physical models, employed by different MC codes [24]-[25].

In this work, the PENELOPE MC code was used to model and simulate the nanodosimetry exercise proposed by the EURADOS group in 2018. The exercise task was to model several and different size of liquid water spheres and perform simulations using the low-energy electron spectrum of ^{125}I radiation source to quantify the energy deposited in the nanoscale sphere targets. Two different types of spectra were proposed to observer the effective cross-sections of the PENELOPE MC code compared to results of other MC codes published in the literature.

2. Method & Materials

2.1. Monte Carlo model

The electron radiation transport was carried out using Penetration and ENErgy LOss of Positrons and Electrons – PENELOPE code version 2018 [26]. The G view program was used to plot the 2-3D geometry of modeled scenario. The electron transport library was provided by PENELOPE/PENGEOM version 2018 [26]. The physics transport parameters used in the simulations were set in two modes, elastic and inelastic collisions. The C1 and C2 parameters are associated to the condensation of electron and positron elastic scattering process. Wcc and Wcr parameters establish the energy frontier between soft and hard radioactive events taking place during both inelastic collision processes, respectively [20],[26]. Thus, for elastic collisions the parameters $C1 = C2 = 0 e Wcc = Wcr = 1 \times 10^8$ were set-up and for inelastic case, the $C1 = C2 = 0.2$ and $Wcc = Wcr = 0$ were used. According to literature, the choice of these specific collision types is intended to reveal the unique contribution of energy deposition on targets to understand the mechanisms underlying biological effects on micro-nanoscale targets [24]. The cut-off energy of 50 eV was set in the simulations and the number of histories were up to 5.0×10^8 resulting in relative uncertainties of up to 2%. The computer running the simulations is equipped with an Intel Core Pentium CPU G4400 @ 3.30 GHz, 8 GB RAM memory, and a 64-bit operating system. Table 1 summarizes the parameters set in the PENELOPE code for the simulations in accord to the Report of American Association of Physicists in Medicine (AAPM) Task-Group 268 [27].

2.2. Case of nanodosimetry

The nanodosimetry scenario provided by the EURADOS group exercise was modeled. Here, the radionuclide source of ^{125}I was placed in a spherical centre of liquid water with a diameter of 10 µm. Other five

Table 1: Checklist of PENELOPE code

Item Name	Code Informations	References
Code, version/year	PENELOPE, 2018	[26]
Cross-sections	Library for electron transport (PENELOPE/PENGEOM)	[26]
Transport parameters	Electrons, cut-off energy = 50 eV for elastic collision ($C1 = C2 = 0, Wcc = Wcr = 1.0\times10^8$) and inelastic collision ($C1 = C2 = 0.2, Wcc = Wcr = 0$)	[20],[26]
Score quantities	Tally Energy Deposition (eV) $v.2012-06-01$	[26]
Number of histories	$\leq 5.0 \times 10^8$ histories	[26]
Relative uncertainty	About 2%	[26]

small spheres (target) with diameters of 3 nm (similar to the size of the DNA double helix) and 8 nm (similar to the size of nucleosomes) were modeled within the liquid water sphere. The target spheres were modeled multiplying by 0, 1, 2, 4 and 8 times the radius of the target (R) from the isotropic point source. Figure 1 shows the schematic view of the model and its 3D representation, using the program G view.

2.3. Spectra used in simulations

Two different energy spectra of ^{125}I were configured and used in the simulations. The spectrum provided by Howell 1992 [28] named as "Config. 1", in which only, the Auger, Coster-Kronig (C.K.) and Internal Conversion (I.C.) electrons decay were considered. The second spectrum named as "Config. 2" was defined by removing the electrons with energy less than 50 eV, since this is the cutoff energy of the PENELOPE code. Table 2 summarizes the electron spectra used in the simulations. The two spectra configured proposed, Config. 1 and 2, were normalized to 100%.

3. Results and Discussions

3.1. Energy deposited

The energy deposited in the liquid water targets 0R, 1R, 2R, 4R, and 8R were calculated. A total of eight simulations were performed, four for each target size of the water sphere (3 nm and 8 nm diameter) and four for the different elastic and inelastic collisions and spectrum (Configs. 1 and 2). Table 3 shows the results and the uncertainties obtained for each target sphere with the different spectra configurations and for the different (Δ (%)) elastic and inelastic collisions. Figure 2 shows the results for the energy deposited in the liquid water target spheres as a function of the distances.

The results obtained were within the uncertainties of up to 2% in all cases studied. The average deviation of the deposited energy computed in the simulations for the two types of collisions and the average deviation of the uncertainties in the target spheres were 2.5% and 21%, respectively. It is possible to observe a larger difference (Δ (%)) of 4.1% for the elastic and inelastic collisions, in the results obtained for the first target sphere (0R) due to its small size. The values of deposited energy calculated in the target spheres decrease as a function of distance from the source in both cases of collisions and the differences (Δ (%)) between the deposited energies in elastic and inelastic collisions decrease as a function of distance from the source up to 4R, which may imply that there is no pattern to the type of collisions due to distances. It also shows that the collisions in this case can be important for 0R, where the source is placed. The average deviation values from the target size of 3-8 nm diameter in Configs. 1 and 2 were 42%, 43%, 48% and 49% for elastic and inelastic collision respectively. In the work of Vilagrasa et al., 2018 [24], the average difference between the target volumes in the range of 3 to 8 nm was about 50% for both collision types, suggesting a possible proportional relationship. In the present work, a similar average value of about 50%

Table 2: Electron spectrum of decay in Auger, C.K. and I.C. electrons from Howell [28]

Radiation	Average energy (eV)	Yield/decay	
		Config. 1	Config. 2
C.K.	6.00E+00	3.66E+00	–
C.K.	2.99E+01	3.51E+00	–
Auger	3.24E+01	1.09E+01	–
C.K.	1.27E+02	1.44E+00	1.44E+00
C.K.	2.19E+02	2.64E-01	2.64E-01
Auger	4.61E+02	3.28E+00	3.28E+00
Auger	3.05E+03	1.25E+00	1.25E+00
I.C.	3.65E+03	7.97E-01	7.97E-01
Auger	3.67E+03	3.40E-01	3.40E-01
Auger	4.34E+03	2.11E-02	2.11E-02
Auger	2.24E+04	1.38E-01	1.38E-01
Auger	2.64E+04	5.90E-02	5.90E-02
Auger	3.02E+04	6.50E-03	6.50E-03
I.C.	3.06E+04	1.10E-01	1.10E-01
I.C.	3.47E+04	2.84E-02	2.84E-02
Total Yield of total electrons per decay		24.9	6.83

was obtained for Config. 2, with the MC code showing greater completeness and performance in detecting low-energy electrons, as expected. It should be noted that at certain distances from the source, particularly at 2R and 4R distances, the energy deposition values for the 3 nm target volumes were higher than those for the 8 nm target volumes. A possible explanation for the observed phenomenon can be attributed to the concept of radioactive equilibrium. This concept states that the absorbed dose at a given point depends on the size of the object relative to the radiation area and the location of the point within the object [3]. In this case, the relatively higher energy deposition values at 3 nm compared to 8 nm targets at 2R and 4R distances can be attributed to the position of the targets. Despite the larger size of the 8 nm targets, their more distant position from the source at the centre results in lower energy deposition compared to the 3 nm targets, which are closer to the source. Interestingly, the difference between the energy deposition values for 3 nm and 8 nm targets decreases significantly at a distance of 8R, indicating that the energy deposition values converge with increasing distance.

3.2. Nth distance law

Based on the values obtained for the targets 1R to 8R, the results of energy deposition obtained in general show a decreasing value according a power law. It is worth noting that the 0R distance was not considered here because it corresponds to the position of the radiation source and its result showed an extremely high value compared to the other target volumes. Therefore, the 1R distance was defined as the first distance and used as a reference value. By normalizing the values to 1R, a graph was created and thus an equation was obtained that corresponds to the recorded values. Figure 2 shows the curve with the corresponding power equation for the simulated cases of elastic collisions in the 3 and 8 nm diameter liquid water targets for configuration 1 and Table 4 shows the values of the parameters calculated in the non-linear regression equation of the curve for each type of collision for both configurations.

It was observed that the power of the equation decreases twofold (parameter b) as the diameter of the liquid water target sphere increases. Furthermore, the curve flattens even more as the diameter of the target increases and the distances consequently increase. The behaviour of these curves is similar to the inverse square of the distance, which also applies at the nanoscale.

Table 3: Energy deposited (eV) and uncertainty for spherical targets of 3 and 8 nm diameter using Monte Carlo code PENELOPE with cross sections for elastic and inelastic collisions.

Spectrum	**D=3nm /Distance**	**0R**	**1R**	**2R**	**4R**	**8R**
Config.1	Elastic Collision	28.5±0.003	0.48±0.0007	0.115±0.0004	0.022±0.0001	0.0049±0.00008
$(E \pm \sigma)$eV	Inelastic Collision	27.3±0.002	0.47±0.0006	0.114±0.0003	0.023±0.0001	0.0051±0.00006
$\Delta(\%)$	$\Delta(E)_{el.-inel.}$	4.1	1.2	0.4	2.9	3.3
	$\sigma(E)_{el.-inel.}$	18	16	14	18	30
Config.2	Elastic Collision	32.9±0.005	1.6±0.001	0.385±0.0007	0.075±0.0003	0.0165±0.0002
$(E \pm \sigma)$eV	Inelastic Collision	29.0±0.004	1.58±0.001	0.382±0.0006	0.078±0.0002	0.0168±0.0001
$\Delta(\%)$	$\Delta(E)_{el.-inel.}$	11.9	1.1	0.8	3.7	1.8
	$\sigma(E)_{el.-inel.}$	22	15	15	16	33
Spectrum	**D=8nm /Distance**	**0R**	**1R**	**2R**	**4R**	**8R**
Config.1	Elastic Collision	42.8±0.005	1.05±0.001	0.0512±0.0003	0.0112±0.0002	0.0062±0.0001
$(E \pm \sigma)$eV	Inelastic Collision	41.6±0.004	1.06±0.001	0.051±0.0002	0.0109±0.0001	0.00626±0.00007
$\Delta(\%)$	$\Delta(E)_{el.-inel.}$	2.9	0.8	0.5	2.6	0.9
	$\sigma(E)_{el.-inel.}$	12	7	27	43	38
Config.2	Elastic Collision	80.9±0.01	3.5±0.003	0.172±0.0007	0.037±0.0004	0.0208±0.0003
$(E \pm \sigma)$eV	Inelastic Collision	76.7±0.01	3.53±0.003	0.169±0.0006	0.036±0.0002	0.0211±0.0002
$\Delta(\%)$	$\Delta(E)_{el.-inel.}$	5.1	0.7	1.6	1.6	1.6
	$\sigma(E)_{el.-inel.}$	0	6	20	34	32
Δ Size	Config.1 $\Delta(E)_{el.}$	33.4	54.7	55.4	49.0	20.9
3-8nm	Config.1 $\Delta(E)_{inel.}$	34.3	55.6	55.2	52.6	18.5
(%)	Config.2 $\Delta(E)_{el.}$	59.3	54.2	55.3	50.6	20.6
	Config.2 $\Delta(E)_{inel.}$	62.1	55.2	55.7	53.8	20.3

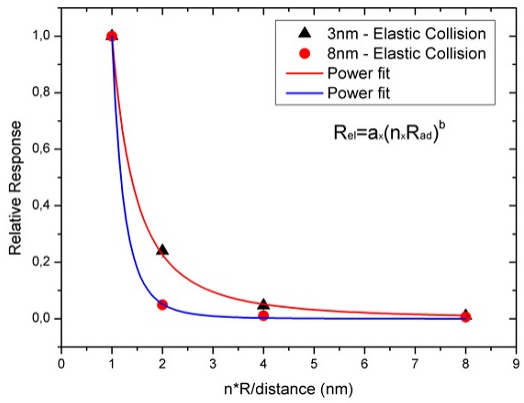

Figure 2: Results of the relative response curve of elastic collisions for 3 and 8 nm in relation to Configuration 1. Plotted curves show the relative response (Rel.) of energy in each spherical target as a function of distance (n*Rad.).

Hoff et al, 2017 [29], presented results obtained for different physical models of the code Geant4- DNA MC for proton transport in nano-layer. In their work, the same curve was observed when the deposited energy was plotted and analyzed as a function of the radius of the nano-layer. The shape of the curve obtained with the code PENELOPE MC was also compared with the Ionization Cluster Size Distribution (ICSD) parameters by Vilagrasa et al. (2018)[24]. The ICSD is the quantification of the ionizations that occur in each medium and can only be calculated using the Monte Carlo code Geant4 [12],[24]. After normalizing the ICSD values obtained for the 1R target, a similar shape of the curve was observed. Figure 3 shows the shape of the curves after normalizing the ICSD parameters in 1R as a function of sphere diameter.

4. Conclusion

This work summarizes the modelling and simulations performed using the PENELOPE MC code, for a case of nanodosimetry using a ^{125}I radiation source. Two different energy spectra, with Auger, C.K. and C.I. electrons were proposed and studied. Two distinct types of collisions, elastic and inelastic, were simulated to understand the deviation of the energy deposited in different 3 and 8 nm diameter liquid water targets spheres. Part of the results were presented and

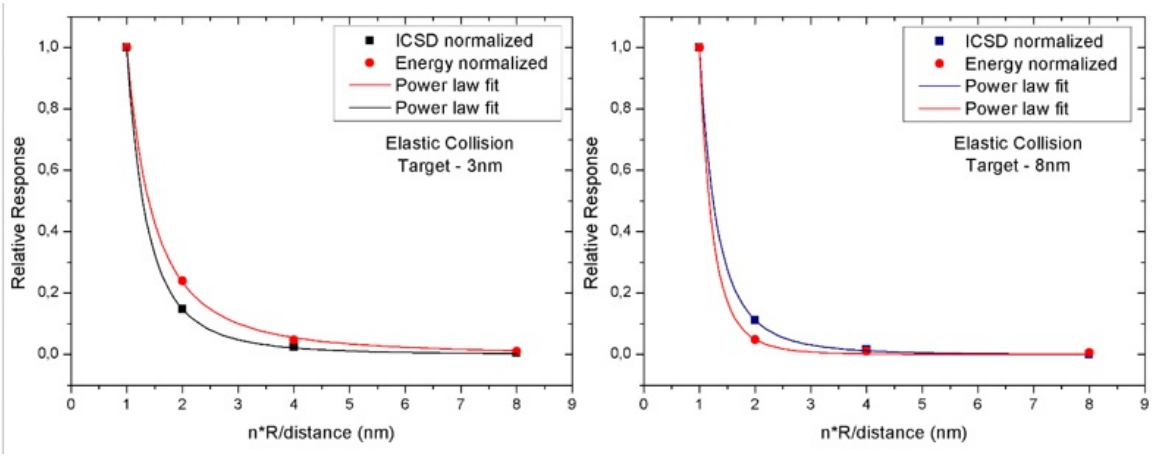

Figure 3: Comparison curve for normalized values for ICSD and energy. Each curve was calculated using power fit regression using Configuration 1.

Table 4: Parameters of the power equation obtained from the nonlinear regression curve for the spherical targets of Configuration 1 and 2, for elastic and inelastic collisions.

Type of Configuration		**Equation Parameter**
	3nm	
Configuration 1	**a**	**b**
Elastic Collision	1.07±0.02	-2.14±0.05
Inelastic Collision	1.00±0.02	-2.13±0.04
Configuration 2	**a**	**b**
Elastic Collision	1.00±0.02	-2.14±0.05
Inelastic Collision	1.00±0.02	-2.13±0.04
	8nm	
Configuration 1	**a**	**b**
Elastic Collision	0.998±0.064	-4.25±0.44
Inelastic Collision	0.995±0.102	-4.21±0.51
Configuration 2	**a**	**b**
Elastic Collision	0.998±0.064	-4.24±0.42
Inelastic Collision	0.995±0.101	-4.22±0.50

further studies should be performed to understand the effects of energy transport for the different MC codes using different low-energy effective cross sections.

Acknowledgements

The following Brazilian institutions support this research project: Research Support Foundation of the State of Minas Gerais (FAPEMIG), Brazilian Council for Scientific and Technological Development (CNPq) and Coordination for the Capacitation of Graduated Personnel (CAPES). L. F. Araújo is grateful for financial support provided by CAPES (Process $n88887.626581/2021 - 00$). Prof. T. C. F. Fonseca is grateful for the financial support provided by CNPq ($424734/2018 - 4$) and FAPEMIG (Project $APQ - 01388 - 21$ Process $n2070.01.0005404/2021 - 81$). We also thank the Computing resources were provided by the scientific computing laboratory of the State University of Rio de Janeiro LCR-UERJ/RJ and Institute of Radiation Protection and Dosimetry - $LN/IRD - CNEN/RJ$.

Authorship contribution

L. F. Araújo (performed and led the simulations in the PE-NELOPE code, discussion results), and T. C. F. Fonseca (discussion results and textual review)

Funding

No funding was received

Conflict of interest

This article has no conflict of interest and the authors have non-financial interests to disclose.

Declaration

This research has been conducted ethically, reporting of those involved in this article.

Similarity Index

I hereby confirm that there is no similarity index in abstract and conclusion while overall is less than 10% where individual source contribution is 2% or less than it.

References

[1] V.C. Thipe, et al. In: U. Shanker, C.M. Hussain, M. Rani (eds) Handbook of Green and Sustainable Nanotechnology. Springer, Cham. (2023). https://doi.org/10.1007/978-3-031-16101-82

[2] B. Sun, C.T. Hagan 4th, J. Caster, A.Z. Wang. Hematol Oncol Clin North Am. 33(6), p. 1071, (2019). https://doi.org/10.1016/j.hoc.2019.08.002. Epub 2019 Oct 1. PMID: 31668207; PMCID: PMC6981287.

[3] F.H. Attix, Introduction to Radiological Physics and Radiation Dosimetry. John Wiley & Sons, p.628, (1991).

[4] J. M. DeCunha, Physics in Medicine & Biology, 66, p.185011,(2021).

[5] A. Papadopoulos, I. Kyriakou Matsuya, Y. Incerti, S. Daglis, I.A. Emfietzoglou, D. Microdosimetry. Appl. Sci., 12, p. 8950. (2022).

[6] A. Baratto-Roldán, A.Bertolet, G.Baiocco, A.Carabe, M. A. Cortés-Giraldo. Frontiers in Physics. Vol. 9, ISSN 2296-424X,(2021).

[7] S. A. Ngcezu, H. Rabus, Radiat Environ Biophys. 60(4), p.559 (2021). https://doi.org/10.1007/s00411-021-00936-4. PMID:34427743; PMCID:PMC8551112

[8] Y. Ali, L. Auzel, C. Monini, K.Kriachok, J. M.Létang, E.Testa, L.Maigne, M.Beuve, Medical Physics. Vol. 49 (5), p.3457 (2022).

[9] Y. Thibaut, N.Tang, H. N.Tran, A.Vaurijoux, C. Villagrasa, S.Incerti, Y.Perrot, Int. J. Mol. Sci. 23, p.3770, (2022).

[10] M. A. Bernal, et al. Physica Medica 31, p.861, (2015).

[11] A. Rucinski, A. Biernacka, R.Schulte, Phys. Med. Biol. 66 p. 24TR01, (2021).

[12] H. Palmans, British Journal of Radiology Vol. 88, p.1045, (2015).

[13] W. B.Li, et al. Radiation Measurements, Vol. 115, p. 29, (2018). https://doi.org/10.1016/j.radmeas.2018.05.013

[14] D. Mazzucconi, et al., Radiation Physics and Chemistry, Vol. 171, p. 108729 (2020). https://doi.org/10.1016/j.radphyschem.2020.108729

[15] L.T. Tran, et al., Appl. Sci. 12, p.328 (2022).

[16] A. Rucinski,, et al. Physics in Medicine & Biology, 66 p.24TR01, (2021).

[17] C.Kirkby, E. Ghasroddashti, Medical Physics 42, p. 1119, (2015).

[18] P. Zygmanski, et al., Phys. Med. Biol. 58, p.7961, (2013).

[19] M. Pietrzak, M.Mietelska, A.Bancer, A. Rucinski, B.Brzozowska, Phys. Med. Biol. 66 p. 225008, (2021).

[20] M. A.Bernal, J. A.Liendo, Med. Phys. 36(2), p.620, (2009).

[21] I. Kyriakou, et al., Applied Radiation and Isotopes, Vol. 172, p. 109654 (2021). https://doi.org/10.1016/j.apradiso.2021.109654

[22] V. M. Markovic, et al. Radiation and Environmental Biophysics, Vol. 59(1), p.161, (2020). https://doi.org/10.1007/s00411-019-00815-z

[23] N. T. Henthorn, et al.,RSC Advances, Vol. 99(12), p. 6845,(2019). https://doi.org/10.1039/C8RA10168J

[24] C. Villagrasa, et al., Radiation Protection Dosimetry. Vol. 183(1-2), p. 11,(2018).

[25] C. Villagrasa, et al., Radiation Measurements. Vol. 150, p. 106675. ISSN: 1350, (2022).

[26] F. Salvat, PENELOPE-2018, OECD Nuclear Energy Agency, (2019).

[27] I. Sechopoulos, et al., Medical Physics, Vol. 45 (1),p. e1–5 (2018). https://doi.org/10.1002/mp.12702

[28] R. W. Howell, Med. Phys. Vol. 19(6),p.1371,(1992).

[29] G. Hoff, et al.,IEEE. 978-1-5386-2282-7, (2017).

Copyright